

Article

Investigation of the Reaction Kinetics of a Sinter-Reduction Process in the Thermal Reserve Zone of a Blast Furnace Using a Modified Sectioning Method

Li Zhu ^{1,2}, Wenlong Zhan ^{3,*}, Yubo Su ³, Yi Liu ³ and Keng Wu ^{2,*}¹ Shougang Research Institute of Technology, Beijing 100041, China; 320143200134@ustl.edu.cn² State Key Laboratory of Advanced Metallurgy, University of Science and Technology Beijing, Beijing 100083, China³ School of Materials and Metallurgy, University of Science and Technology Liaoning, Anshan 114000, China; 202085600292@stu.ustl.edu.cn (Y.S.); 202085600275@stu.ustl.edu.cn (Y.L.)

* Correspondence: zhanwenlong@ustl.edu.cn (W.Z.); wukeng@metall.ustb.edu.cn (K.W.)

Abstract: With the development of large-scale and high-performing blast furnaces, it is necessary to extensively study the reaction characteristics and related kinetic parameters of sinters in their heat reserve area. Under reducing atmosphere conditions, the reduction of iron oxide in sinter is closely related to the gasification reaction of coke. Based on a simulation experiment, the transition point from chemical reactions to diffusion and the related kinetic parameters were determined through a sectioning method. The results showed that increasing the proportion of low-grade coke increased the chemical-reaction rate, but it slightly decreased the mass-transfer and diffusion rates. An increase in the coke particle size increased the chemical-reaction, mass-transfer, and diffusion rates. However, an increase in the CO₂ volume fraction in gas reduced the chemical-reaction, diffusion, and mass-transfer rates. The mixing ratio of coke and sinters increased the chemical-reaction rate, but it decreased the mass-transfer and diffusion rates. The rate constant of the chemical reactions in the early stage was three orders of magnitude higher than that of the diffusion and mass-transfer coefficients, and the fitting degree was obviously better than that of the molecular diffusion in the later stage. Based on the thermodynamics of irreversible processes, the interference of the chemical reactions with the diffusion and mass transfer in the near-equilibrium region was tentatively established, the method of controlling coke diffusion and mass transfer in the later reaction stage was given and related kinetic parameters were corrected, and further improvement of the modified sectioning method was completed.

Keywords: sinter reduction; blast furnace; modified sectioning method; irreversible process thermodynamics; near-equilibrium region



Citation: Zhu, L.; Zhan, W.; Su, Y.; Liu, Y.; Wu, K. Investigation of the Reaction Kinetics of a Sinter-Reduction Process in the Thermal Reserve Zone of a Blast Furnace Using a Modified Sectioning Method. *Metals* **2022**, *12*, 1259. <https://doi.org/10.3390/met12081259>

Academic Editor: Alexander McLean

Received: 6 June 2022

Accepted: 24 July 2022

Published: 26 July 2022

Publisher's Note: MDPI stays neutral with regard to jurisdictional claims in published maps and institutional affiliations.



Copyright: © 2022 by the authors. Licensee MDPI, Basel, Switzerland. This article is an open access article distributed under the terms and conditions of the Creative Commons Attribution (CC BY) license (<https://creativecommons.org/licenses/by/4.0/>).

1. Introduction

Steel production in China mainly depends on the melting of iron using blast furnaces, in which iron-containing sinters are mainly used as charge materials. The reducibility of these sinters directly affects the productivity and fuel ratio, and depends on many factors such as chemical composition, alkalinity, porosity, and mineral composition [1–4]. Many studies have been conducted on the reaction kinetics of sinters under different gas conditions. Among them, El-Geassy [5] clarified the rate-controlling step in the reduction process using the values of the apparent activation energy. The early stage of reduction was considered to be controlled by the combined effects of gaseous diffusion and interfacial chemical reactions. Murakami [6] further evaluated the effects of H₂ and H₂O gases on the disintegration of iron ore sinter in a blast furnace. However, only a few studies have investigated the reaction kinetics of the reduction of iron-containing oxides in the

isothermal block zone of blast furnaces in the presence of different coke and reducing gas components [7].

One of the characteristics of metallurgical reaction kinetics is its greater dependence on the mechanism of the reaction rather than on the rate of the entire multiphase process. The reduction of iron ore is composed of different rate-controlling processes such as gas external diffusion, internal diffusion, and chemical reactions, among which chemical reactions have the slowest rate [8–12]. However, these findings are semiquantitative because the transition points of different rate-controlling processes at the early and later stages and the relevant kinetic parameters cannot be obtained from reaction simulations. One of the main objectives of research studies on metallurgical reactions is to simulate metallurgical processes to determine reaction mechanisms using kinetic parameters. In order to perform simulations of metallurgical processes, it is necessary to establish a new method suitable for metallurgical reactions.

In this paper, sinter-reduction kinetics in the thermal reserve zone of a blast furnace were studied through a sectioning method. Based on mass-transfer and chemical-reaction mechanisms, the chemical-reaction and diffusion models of different reduction stages were established. In addition, the kinetic parameters and transition points of different rate-controlling processes involved in sinter reduction were determined based on experimental data.

Sinter reduction was dominated by chemical reactions and diffusion at the early and later stages, respectively, as determined through a sectioning method; whereas in actual sinter reduction, chemical reactions, diffusion, and mass transfer simultaneously occur [13–15]. The rate of chemical reactions was several orders of magnitude higher than that of diffusion and mass transfer, and the fitting degree between a chemical-reaction model and a test point was obviously better than that between a diffusion and mass-transfer model. Based on the thermodynamics of irreversible processes, in the near-equilibrium region of sinter reduction, the effect of chemical reactions on the interference or coupling of diffusion and mass-transfer processes was established; the chemical, diffusion, and mass-transfer coefficients in the late- and near-equilibrium regions were determined, the fitting degree between the diffusion and mass-transfer model and the test point was improved, and the sectioning method suitable for metallurgical reactions was further improved.

The coupling reaction among coke, CO, CO₂, and iron oxides exist during sinter reduction in the thermal reserve zone of blast furnaces [16–19]. During reduction of iron oxides, the oxygen atom from iron oxides and carbon atom from coke generate CO and CO₂. In this experiment, the CO and CO₂ concentrations and total weight loss of carbon in the coke, as well as the oxygen in iron oxides, were measured based on gas composition and mass conservation, respectively. These data were necessary for the study of reaction kinetics.

2. Materials and Methods

2.1. Materials

In the experiment, iron oxides in sinter were reduced step by step. Sinter reduction was simulated in the presence of coke in the heat reserve lump zone of a hanging high-temperature blast furnace under reducing atmosphere conditions. Simultaneously, FeO reduction ($\text{FeO} + \text{C} = \text{Fe} + \text{CO}$) occurred when CO₂ in the off-gas reacted with carbon in the coke to form CO [20–23]. The sinter and coke were first dried in a drying oven for 2 h at 100 °C. Afterward, a hanging basket made of iron wire containing the coke and sinter mixed in certain proportions was placed inside the high-temperature furnace, which was heated to 1000 °C at a suitable heating rate. Then, CO, CO₂, and N₂ gas mixed at certain proportions was introduced into the furnace at a total flow rate of 10 L/min until the end of the experiment. In the thermal reserve lump zone of the blast furnace, FeO was reacted with CO to form Fe and CO₂. Finally, the blast furnace was cooled from 1000 °C to room temperature by switching the mixed gas to N₂ at a flow rate of 5 L/min after the simulated sinter reduction was finished.

The composition and metallurgical property of the coke and sinter used in the experiment are shown in Tables 1 and 2, respectively.

Table 1. Metallurgical property and component of cokes (wt%).

Cokes	M40	M10	CSR (Coke Strength after Reaction)	CRI (Coke Reactivity Index)	Ash	Volatile	Moisture	S
Coke A	83.3	6.5	67.7	22.6	12.8	0.88	1.3	0.75
Coke B	78.2	7.6	60.3	29.9	13.1	1.27	9.0	0.80
Coke C	81.8	7.5	57.9	31.9	13.2	1.08	10	0.79

Table 2. Chemical composition of sinter (wt%).

Composition	TFe	TMn	FeO	SiO ₂	TiO ₂	MgO	CaO	Al ₂ O ₃
Percentage	51.49	0.22	8.63	7.47	0.17	2.00	14.81	2.12

2.2. Methods

(1) Methods for sinter reduction

Using an electronic balance, the weight loss of the sinter and coke during reduction was measured. The inflow of CO, CO₂, and N₂ was controlled using mass flow meters, and the composition (mainly CO and CO₂) of the off-gas emitted from the furnace was continuously measured using an infrared gas analyzer. The simulation experiment setup is shown in Figure 1.

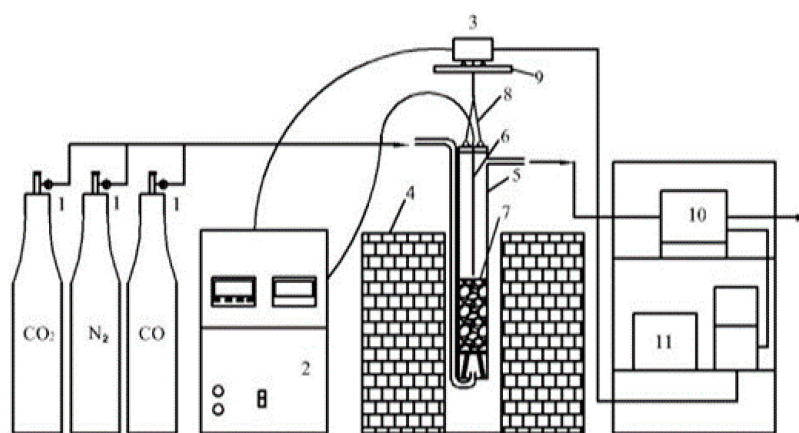


Figure 1. Schematic diagram of hanging high-temperature furnace for simulation experiment. 1—mass flow meter; 2—temperature-controlling instrument; 3—electronic balance; 4—heating furnace; 5—hanging high temperature furnace; 6—thermocouple; 7—test specimen; 8—hanging chain; 9—cradle support; 10—gas analyzer; 11—computer.

Table 3 shows the experimental schemes for the simulated sinter reduction under different conditions; the parameters of the sinter were kept unchanged in these experiments, with the granularity between 10 and 12.5 mm. In the first, second, third, and fourth experimental schemes, different types of metallurgical coke, different proportions of CO and CO₂, different particle sizes of coke, and different charging methods were used, respectively.

Table 3. Experimental schemes of sinter reduction kinetics.

Sample No.	N ₂	Gas Ratio %		Granularity /mm	Sinter	BF Materials/g			Charging Method	
		CO	CO ₂			Coke A	Coke B	Coke C		
1	1-1	70	30	0	10–15	180	45	45	0	Mixed charging
	1-2	70	30	0	10–15	180	45	22.5	22.5	Mixed charging
	1-3	70	30	0	10–15	180	45	15	30	Mixed charging
2	2-1	60	35	5	10–15	180	45	22.5	22.5	Mixed charging
	2-2	60	30	10	10–15	180	45	22.5	22.5	Mixed charging
	2-3	60	25	15	10–15	180	45	22.5	22.5	Mixed charging
3	3-1	70	30	0	10–15 (coke A) 6–9 (coke B and coke C)	180	45	22.5	22.5	Mixed charging
	3-2	70	30	0	10–15 (coke A) 9–12 (coke B and coke C)	180	45	22.5	22.5	Mixed charging
	3-3	70	30	0	10–15 (coke A) 12–15 (coke B and coke C)	180	45	22.5	22.5	Mixed charging
4	70	30	0	10–15	180	45	22.5	22.5	Layer charging	

(2) Methods for analyzing the interference of chemical reactions with diffusion in the near-equilibrium region by irreversible thermodynamics

In complex metallurgical processes, various chemical reactions and material transfers are simultaneously carried out; that is, there is a mutual “coupling” of various chemical reactions, mass transfer, heat transfer, fluid flow, conductivity, and other physical processes. To study the transport phenomena in the thermodynamics of irreversible processes, it is necessary to determine not only the relationship between the transport flux and its driving force, but also the “interference effect” when more than two irreversible processes are coupled [24].

In the thermodynamics of irreversible processes, the entropy of per unit volume and per unit time is defined as the entropy increase rate, which can be written as the following general formula:

$$\sigma = \sum_{i=1}^n J_i X_i \quad (1)$$

where σ represents the entropy increase rate, J_i represents type i of thermodynamic flux, and X_i represents type i of thermodynamic force.

For open systems, macroscopic irreversible processes begin when the boundary conditions force the system to leave the equilibrium state. Because the flux in irreversible processes is dependent on force, it can be considered that the functional relationship between flux and force is as follows:

$$J_i = f(X_1, X_2, \dots, X_n) \quad (i = 1, 2, \dots, n) \quad (2)$$

Based on the experiments conducted, it was established that the interference in irreversible processes in the system was coupling. When a phenomenological equation is applied to the interference of different processes, the coupling constraints of different forces and different fluxes should be considered first. The spatial characteristics of different forces and different fluxes may be completely different. For example, some forces and fluxes are scalars that are zero-order tensors, and some are vectors that are first-order tensors. However, tensors are usually of the second order. When the phenomenological equation is described by the entropy increase rate, force and flux must be the tensors with the same order; that is, to meet Curie’s law [25]. According to Curie’s isotropic medium, force and flux with different order tensors cannot be coupled; for example, when the force of chemical reactions is scalar, but the heat flow and material flow are vectors. As isotropic media, they cannot be coupled when the chemical reactions are far from equilibrium. Similarly, vector forces such as temperature gradient and concentration gradient cannot be coupled with scalars such as the chemical-reaction rate.

When the concentration distribution of components in the system is not uniform, there is a diffusion flow caused by the concentration (or chemical potential) gradient at each spatial position (x , y , and z) in the system. The concentration of each element at each point will be affected by the diffusion and chemical reactions if chemical reactions exist in the system. If there is only one chemical reaction (or only one reaction related to component i) in the system, the mass-conservation equation is given by the following formula:

$$\rho \frac{\partial c_i}{\partial t} = v_i J - \nabla \cdot \vec{J}_i \quad (3)$$

where J is the rate of chemical reactions. Based on the assumption in thermodynamics of the functional relationship between flux and force in irreversible processes, J can be calculated as follows [26]:

$$J = f\left(-\frac{A}{T}\right) \quad (4)$$

Equation (5) is derived using the Taylor expansion in Equation (4), which is shown as follows:

$$J = \left[L_1 \frac{A}{T} + L_2 \left(\frac{A}{T}\right)^2 + L_3 \left(\frac{A}{T}\right)^3 + \dots \right] \quad (5)$$

where L_i is the phenomenological coefficient and A is the affinity, which is the chemical potential difference between products and reactants.

In general, it is believed that diffusion satisfies Fick's law, and that the diffusion coefficient is a constant. If the coupling of each component diffusion flow is ignored, Equation (3) can be written as follows:

$$\rho \frac{\partial c_i}{\partial t} = v_i J - L_{ii} \nabla^2 \left(\frac{\mu_i}{T}\right) \quad (6)$$

Formula (7) can be obtained by substituting Formula (5) into Formula (6), as follows:

$$\rho \frac{\partial c_i}{\partial t} = -v_i \left[L_1 \frac{A}{T} + L_2 \left(\frac{A}{T}\right)^2 + L_3 \left(\frac{A}{T}\right)^3 + \dots \right] - L_{ii} \nabla^2 \left(\frac{\mu_i}{T}\right) (i = 1, 2, \dots, n) \quad (7)$$

3. Results and Discussions

3.1. Experimental Data Processing

Figure 2 shows the changes in the total weight loss in the second group experiment and the corresponding composition of the off-gas discharged from the furnace during the experiment.

The total weight loss of the sinter and coke in the second experimental scheme is shown in Figure 2a including a loss in oxygen atoms from the iron oxide in the sinter and a loss in carbon atoms from the coke during the reaction. During the entire reduction process, the off-gas composition continually changed because carbon reacted with CO_2 to generate CO, and the sinter reduction in the lump zone of the blast furnace could not reach equilibrium, as shown in Figure 2b.

The changes in the amount of oxygen and carbon in the off-gas came from iron oxide in the sinter and carbon in the coke, respectively. First, the proportions of carbon and oxygen were calculated according to the changes in the proportions of CO and CO_2 in the off-gas during the reaction, and then the losses in the weights of carbon and oxygen at any moment could be determined according to the total weight loss. According to the theory of step-by-step reduction, the sinter reduction in the blast furnace mainly involved the reduction of FeO. The weight-loss rate of FeO could be calculated based on the loss in weight of oxygen at any moment. Figure 3 shows the weight-loss curves during the simulated sinter-reduction experiments.

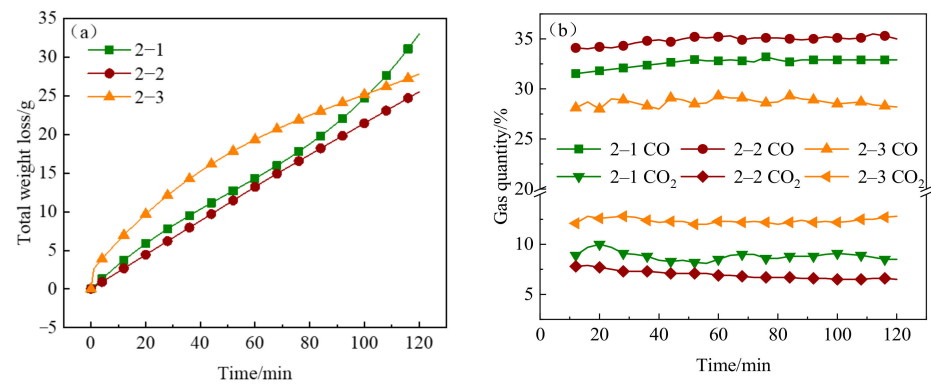


Figure 2. Weight loss in the second group experiment and corresponding gas compositions. (a) Total weight loss curve during experiment; (b) gas compositions emitted during experiment.

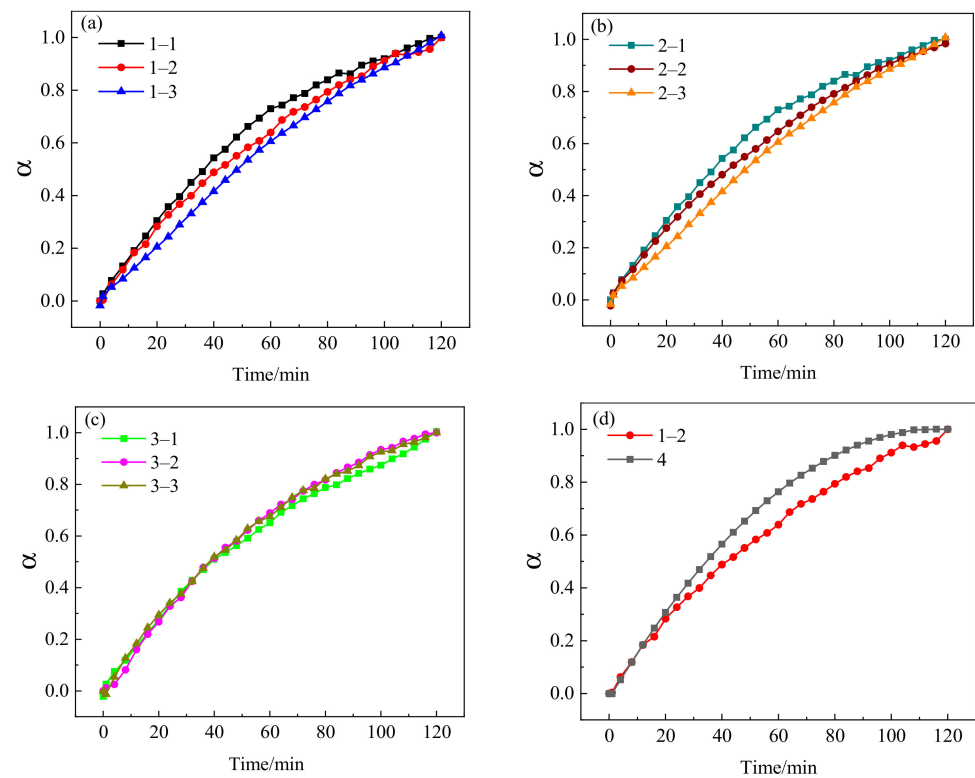


Figure 3. Mass-loss curves of sinter in experiments. (a) First group experiment; (b) second group experiment; (c) third group experiment; (d) fourth group experiment.

In the first experimental scheme, the proportion of coke A remained unchanged, the proportion of coke B gradually decreased, and the proportion of coke C increased. Therefore, the proportion of low-quality coke gradually increased, and the corresponding weight-loss rate of the sinter slightly decreased, indicating that the increase in the low-quality coke proportion would have a negative impact on the reduction of the sinter. A small amount of low-quality coke in iron production could reduce the cost of the pig iron, but the amount of low-quality coke should be limited. Otherwise, the reduction of sinter could be greatly affected. In the second experimental scheme, the effect of CO₂ on the conversion rate of the sinter was analyzed. The conversion rate of the sinter decreased with an increasing CO₂ content in the off-gas, which had an adverse effect on the reduction of the sinter, as shown in Figure 3b. In the third experimental scheme, the effect of different particle sizes of the low-quality coke was analyzed. The selected range of coke particle sizes had a small effect on the conversion rate of the sinter, which was related to the

changes in coke particle size, as shown in Figure 3c. In the fourth experimental scheme, the effect of different charging modes on the sinter conversion was determined, as shown in Figure 3d. The sinter conversion rate of the layer-charging mode was higher than that of the mixed-charging mode, which was caused by the large porosity and good permeability of the coke layer.

The above discussion was only a qualitative analysis of the effects of different coke parameters on sinter reduction, but the reaction process also could be quantitatively analyzed via calculation of the kinetic parameters.

3.2. Kinetics Model of Iron Oxide Reduction of the Sinter

At the initial stage of sinter reduction in the upper part of the blast furnace, the gas flow and temperature are high, and external diffusion will generally not become a restrictive process. At this time, the formation of a product layer is fast, and internal diffusion will not become a restrictive process [27,28]. In the later stage of the reaction, due to the reduction of unreacted nuclei and the increase in product layer thickness, the diffusion of gas in the solid phase will become a restrictive process [29].

In the upper thermal reserve lump zone of the blast furnace, the reduction from FeO to Fe adopted the unreacted nuclear model, which was controlled by chemical reactions in the early stage of the reduction process; its integral formula was as follows:

$$1 - (1 - \alpha)^{\frac{1}{3}} = \frac{k_{\text{rea}} C_0 M}{\rho r_0} t = Kt \quad (8)$$

where α is the reaction rate, which is the weight loss of the sinter at different times divided by the total weight loss of the sinter; k_{rea} is the reaction-rate constant in moles per second; C_0 is the molar volume of FeO in moles per cubic meters; M is the molar mass of Fe in kilograms; t is the reaction time in seconds; r_0 is the equivalent radius of the sinter reaction core in meters; ρ is the density of the sinter in kilograms per cubic meter; and $K = (k_{\text{rea}} C_0 M) / (\rho r_0)$.

In Equation (8), $(1 - (1 - \alpha)^{1/3})$ could be fitted with the reaction time t to obtain the linear slope K , which could be substituted into Equation (9) to calculate the chemical-reaction-rate constant k_{rea} :

$$k_{\text{rea}} = \frac{K \rho r_0}{C_0 M} = \frac{K \rho r_0}{(W_0 / M V_0) M} = \frac{K \rho r_0}{(W_0 / V_0)} \quad (9)$$

where W_0 is the mass of the sinter in kilograms before the reaction and V_0 is the volume in cubic meters before the reaction.

In the upper thermal reserve lump zone of the blast furnace, the reduction of FeO to Fe in the sinter was controlled by internal diffusion at the later stage of the reaction; its integral formula was as follows:

$$\left(1 - \frac{2}{3}\alpha - (1 - \alpha)^{\frac{2}{3}}\right) = K't \quad (10)$$

where $K' = \frac{2D_{\text{ABP}}(C_0 - C_i)M}{\rho r_0^2}$.

At the later stage of the reduction of FeO present in the sinter, the linear slope K' could be obtained by fitting $(1 - 2\alpha/3 - (1 - \alpha)^{2/3})$ in Equation (3) with time t , and then the molecular diffusion coefficient D_{ABP} at the later stage of the reaction could be calculated:

$$D_{\text{ABP}} = \frac{\rho r_0^2 K'}{2(C_0 - C_i)M} \quad (11)$$

3.3. Fitting Results of Kinetics Model Obtained through the Sectioning Method

According to the weight-loss rates of the sinter in different experiments as shown in in Figure 3, $(1 - (1 - \alpha)^{1/3})$ in Equation (1) and $(1 - 2\alpha/3 - (1 - \alpha)^{2/3})$ in Equation (3) were fitted with t through the sectioning method, and then the slope K and K' were determined. The segment point of the segment fitting corresponding to the maximum value of the sum of the two fitting correlation coefficients was adopted as the optimum segment point. If the maximum value of the sum of the two fitting correlation coefficients was the same, the segment point of the segment fitting corresponding to the maximum value of reaction correlation coefficient at the early stage was adopted as the optimum segment point.

Table 4 shows the linear fitting equations and correlation coefficients obtained by the chemical-reaction model at the early stage and the internal diffusion model at the later stage of sinter reduction in different experiments in the upper thermal reserve lump zone of the blast furnace through the sectioning method. Figure 4 shows the segment point of the segment fitting and the linear fitting results at the early chemical-reaction control stage and at the later internal-diffusion control stage.

Table 4. Linear fitting equation and correlation coefficients at different stages.

Sample No.	Chemical-Reaction Model at the Early Stage		Internal-Diffusion Model at the Later Stage		
	Linear Fitting Equation	Correlation Coefficient r_1	Linear Fitting Equation	Correlation Coefficient r_2	
1	1-1	$y = 0.000985x + 0.0543$	0.9929	$y = 0.000778x + 0.0496$	0.9823
	1-2	$y = 0.000789x + 0.0378$	0.9894	$y = 0.000806x + 0.0576$	0.9802
	1-3	$y = 0.000650x + 0.0347$	0.9974	$y = 0.000838x + 0.0555$	0.9873
2	2-1	$y = 0.000535x + 0.0315$	0.9923	$y = 0.001410x + 0.0848$	0.9848
	2-2	$y = 0.000529x + 0.0271$	0.9921	$y = 0.000901x + 0.0588$	0.9835
	2-3	$y = 0.000508x + 0.0367$	0.9929	$y = 0.000677x + 0.0450$	0.9878
3	3-1	$y = 0.000894x + 0.0502$	0.9931	$y = 0.000803x + 0.0509$	0.9906
	3-2	$y = 0.000931x + 0.0577$	0.9936	$y = 0.000806x + 0.0459$	0.9824
	3-3	$y = 0.000943x + 0.0423$	0.9943	$y = 0.000745x + 0.0515$	0.9825
4	$y = 0.001250x + 0.0641$	0.9947	$y = 0.000834x + 0.0569$	0.9832	

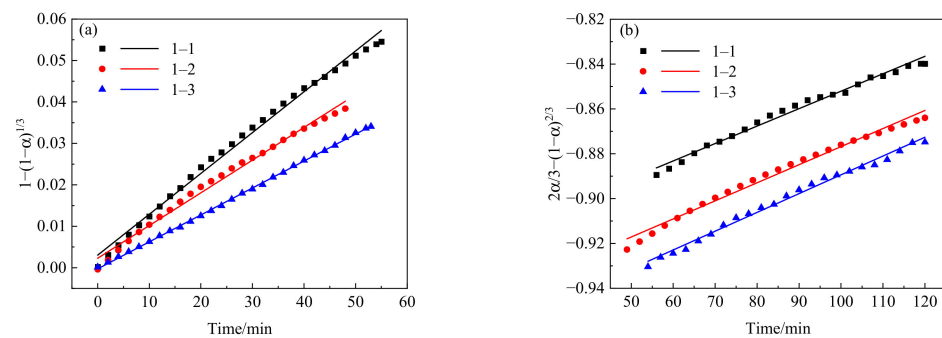


Figure 4. Cont.

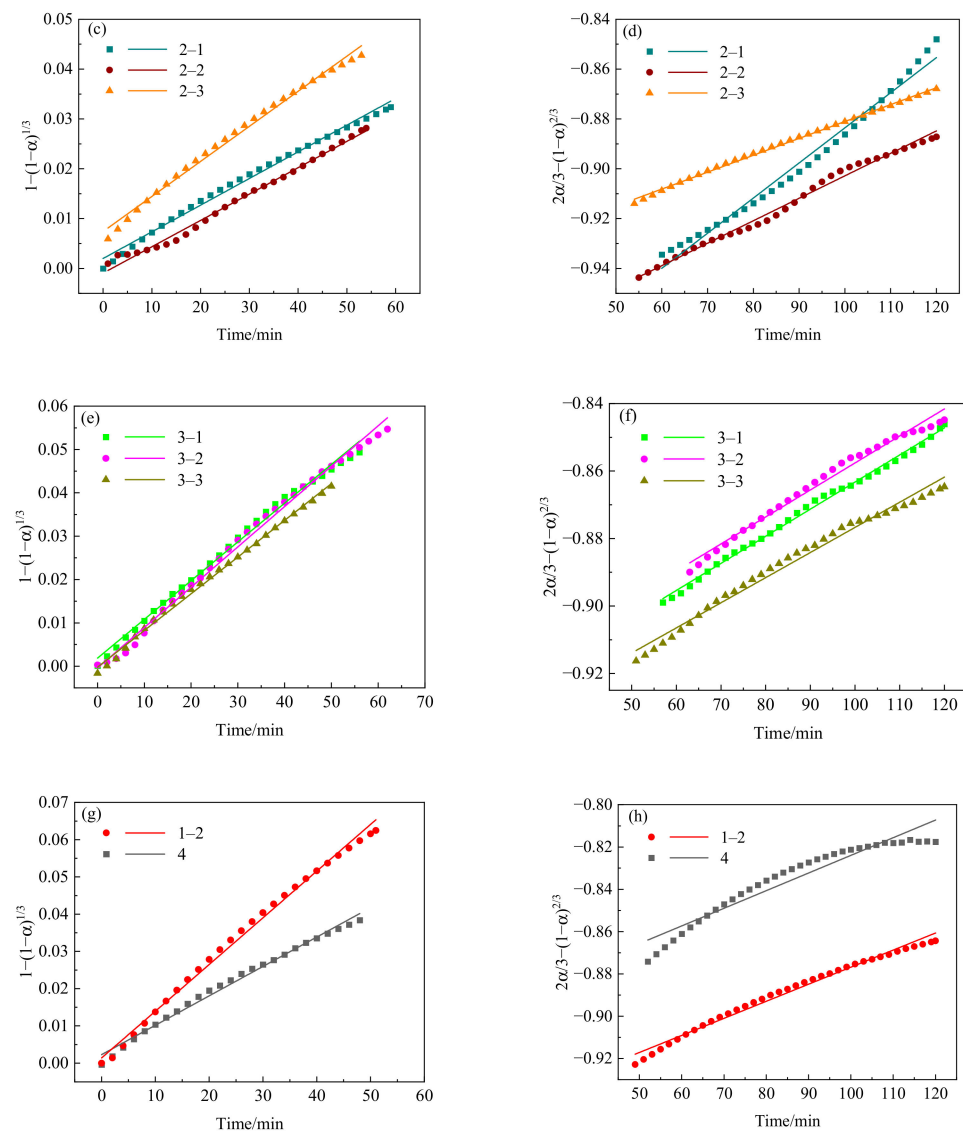


Figure 4. Fitting results of sectioning method. (a) Chemical-reaction speed control of the first group experiment; (b) Internal-diffusion control of the first group experiment; (c) chemical-reaction speed control of the second group experiment; (d) internal-diffusion control of the second group experiment; (e) chemical-reaction speed control of the third group experiment; (f) internal-diffusion control of the third group experiment; (g) chemical-reaction speed control of the fourth group experiment; (h) internal-diffusion control of the fourth group experiment.

Table 4 shows that the early mode established by the sectioning method could linearly fit well with the experimental data, since most of the corresponding correlation coefficients were higher than 0.9900, except for the experimental scheme 1-2, which had a correlation coefficient of 0.9894. However, the later mode established by the sectioning method fit poorly with the experimental data, and its corresponding correlation coefficients were in the range of 0.9802–0.9909. It was proved that the first-order interfacial chemical-reaction-rate control model at the early stage and the shrinkage core internal diffusion rate control model at the later stage were suitable for the reaction kinetics of the sinter in the upper heat reserve lump zone of the blast furnace.

3.4. Kinetics Parameters of Sinter Reduction

When the slopes of the linear fitting equation of the early chemical-reaction-rate control model and later internal diffusion rate control model in Table 4 were substituted

into Equations (8) and (10), respectively, the chemical-reaction-rate constants at the early stage, the internal-diffusion coefficients at the later stage, and the segment point of the two control processes could be calculated in the different experiments. The kinetic parameters of the sinter reduction at the early and later stages are shown in Tables 5 and 6, respectively.

Table 5. Chemical-reaction kinetics parameters during sinter-reduction process at the early stage.

Sample No.		Total Reaction Time/s	Chemical-Reaction Control Time/s	Time Proportion of Chemical-Reaction Control/%	F_1	Slope/ tf	Reaction Velocity Constant $k_{rea}/m \cdot s^{-1}$
1	1-1	7200	3300	45.83	0.0543	0.000985	3.81×10^{-3}
	1-2	7200	2880	40.00	0.0378	0.000789	3.05×10^{-3}
	1-3	7200	3180	44.16	0.0347	0.000650	2.51×10^{-3}
2	2-1	7200	3540	49.16	0.0315	0.000535	2.07×10^{-3}
	2-2	7200	3240	45.00	0.0271	0.000529	2.04×10^{-3}
	2-3	7200	3180	44.16	0.0253	0.000508	2.01×10^{-3}
3	3-1	7200	3360	46.66	0.0502	0.000894	3.46×10^{-3}
	3-2	7200	3720	51.66	0.0577	0.000931	3.60×10^{-3}
	3-3	7200	3000	41.66	0.0593	0.000943	3.84×10^{-3}
4		7200	3060	42.50	0.0641	0.001250	4.84×10^{-3}

Table 6. Internal-diffusion kinetics parameters during sinter-reduction process at the later stage.

Sample No.		Total Reaction Time/s	Internal-Diffusion Control Time/s	Time Proportion of Internal-Diffusion Rate Control %	F_2	Slope/ B	Molecular-Diffusion Coefficient $D_{ABP}/(m^2 \cdot s^{-1})$
1	1-1	7200	3900	54.17	0.0496	0.000778	1.73×10^{-6}
	1-2	7200	4320	60.00	0.0576	0.000806	1.82×10^{-6}
	1-3	7200	4020	55.84	0.0555	0.000838	1.89×10^{-6}
2	2-1	7200	3660	50.84	0.0848	0.001410	1.85×10^{-5}
	2-2	7200	3960	55.00	0.0588	0.000901	3.83×10^{-6}
	2-3	7200	4020	55.84	0.0450	0.000677	3.75×10^{-6}
3	3-1	7200	3840	53.34	0.0509	0.000803	1.30×10^{-6}
	3-2	7200	3480	48.34	0.0459	0.000806	1.39×10^{-6}
	3-3	7200	4200	58.34	0.0520	0.000845	1.43×10^{-6}
4		7200	4140	57.50	0.0569	0.000834	1.15×10^{-6}

In the first experimental scheme shown in Table 5, the chemical-reaction-rate constant significantly decreased with an increase in the low-quality coke proportion. This suggested that the increase in the low-quality coke proportion was not a disadvantage for the sinter reduction in the upper thermal reserve lump zone of the blast furnace. The molecular-diffusion coefficient at the later stage slightly increased because the increase in the low-quality coke proportion had a small effect on the diffusion at the later stage of sinter reduction, as shown in Table 6. In the second experimental scheme shown in Tables 5 and 6, the chemical-reaction-rate constant slightly decreased and the molecular-diffusion coefficient significantly decreased with an increasing CO₂ ratio in the off-gas because the increase in the CO₂ ratio in the off-gas had a significant effect on the gasification reaction of the coke and a less-significant effect on the sinter reduction. In the third experimental scheme shown in Tables 5 and 6, the chemical-reaction rate and molecular-diffusion coefficient slightly increased with an increasing particle size of the low-quality coke. This suggested the increase in the coke particle size was beneficial to the sinter reduction in the upper thermal reserve lump zone of the blast furnace.

By comparing experimental scheme 1-2 with experimental scheme 4 shown in Tables 5 and 6, it was found that the chemical-reaction-rate constant of the layer charging was higher than that

of the mixed charging. In addition, the molecular-diffusion coefficient of the layer charging was lower than that of the mixed charging, probably because the coke porosity of layer charging was larger than that of the mixed charging, which was beneficial to the gasification reaction of the coke. Therefore, carbon monoxide could be rapidly generated to accelerate the reaction rate of the sinter reduction. It is known that the porosity of single-granularity materials is smaller than that of multigranular ones. Therefore, the sinter porosity of the layer charging was smaller than that of the mixed charging, and the molecular-diffusion coefficient during the sinter reduction slightly decreased at the later stage.

When there were small changes in temperature, the changes in the pre-exponent factor A , reaction-activation energy E_0 , and corresponding chemical-reaction-rate constant in the Arrhenius equation $k_{\text{rea}} = A \exp(-E_0/RT)$ were small. Similarly, the changes in the standard-state diffusion coefficient D_0 , diffusion-activation energy E , and corresponding diffusion coefficient in the Arrhenius equation $D_{AB} = D_0 \exp(-E/RT)$ were small. It was considered that the pre-exponent factor A and activation energy E_0 were the constants in the Arrhenius formula governing the thermal reserve zone of the blast furnace. Therefore, other reaction-rate constants on the temperature fluctuations in the thermal reserve zone could be calculated based on the reaction-rate constants at 1000 °C.

4. Sectioning Method Considering the Interference of Chemical Reactions with Diffusion

4.1. Interference of Chemical Reactions with Diffusion in the Near-Equilibrium Region

In the block zone heat reserve area at the upper part of the blast furnace, the reduction of FeO present in the sinter could be determined as the control process through the sectioning method. This area was far from equilibrium, and in this area, chemical reduction was a zero-order tensor, while molecular diffusion and mass transfer were first-order tensors. According to Curie's law, there can be no coupling between different tensors. Therefore, in the early stage of FeO reduction, the interference of molecular diffusion with chemical reactions did not need to be considered. This was completely consistent with the fact that the chemical-reaction-rate constant obtained by the sectioning method was three orders of magnitude higher than most of the molecular diffusion coefficients, as shown in Tables 5 and 6. Considering the interference of the molecular diffusion with the chemical reactions was meaningless.

At the later stage of FeO reduction, molecular diffusion was the control process. The region was within the approximate equilibrium, where chemical reactions and molecular diffusion should have the same order tensors. Therefore, coupling between chemical reactions and diffusion existed; namely, the interference of chemical reactions with molecular diffusion needed to be considered, which did not violate Curie's law. In the near-equilibrium region, the effect of chemical-reaction interference was not necessarily linear; thus, it was necessary to choose a high-order polynomial and analyze the relevant effect through experiments.

Because it is not necessary to consider the interference of molecular diffusion with chemical reactions when they are far from equilibrium (early stage of the reaction), but to consider the effect of chemical reactions on diffusion interference when they are near equilibrium (late stage of the reaction), Onsager's theorem is not suitable for the mutual coupling of chemical reactions and diffusion because their coupling matrix is asymmetric.

According to phenomenological equation, referring to the mutual coupling of heat transfer and mass transfer, such as the interference of heat transfer with mass transfer via the Solett effect and Duvu effect, the coupling equation of the interference of a single chemical reaction on molecular diffusion in the near-equilibrium region was proposed as follows:

$$J_W = \frac{\partial c_i}{\partial t} = -D_e \text{grad}c - v_i \left[L_{1m} \frac{A_m}{T} + L_{2m} \left(\frac{A_m}{T} \right)^2 + L_{3m} \left(\frac{A_m}{T} \right)^3 + \dots \right] \quad (12)$$

where J_w is the diffusion flux and L_{1m} , L_{2m} , and L_{3m} are the mutual phenomenological coefficients considering the coupling of a chemical reaction and diffusion.

In Equation (12), the first and second items could be obtained by conducting a sinter-reduction experiment. The third term, which represents diffusion and mass transfer at the later stage of the reduction of sinter, could be calculated using Equation (10) through the sectioning method. The fourth term, which represents the interference of the chemical reaction on molecular diffusion, could be determined via the difference between the experimental value of the reaction at the later stage and the calculated value when using Equation (10) through the sectioning method. At the same time, a high-order polynomial and its corresponding phenomenological coefficient could be determined according to the accuracy requirement.

4.2. Equation of Interference of Chemical Reactions with Molecular Diffusion during Sinter Reaction

As shown in Figure 3a,c,e,g, the fitting lines of chemical reactions at the early stage were in good agreement with the experimental data. On the other hand, as shown in Figure 3b,d,f,h, the fitting lines of molecular diffusion at the later stage were in relatively poor agreement with the experimental data, and some had greater differences. The correlation coefficient at the early stage was also higher than the corresponding correlation coefficient at the later stage, as shown in Table 4.

Supposing there was no interference of chemical reactions with molecular diffusion in the near-equilibrium region, the fitting lines of molecular diffusion at the later stage should have been in good agreement with the experimental data in Figure 3b,d,f,h. In fact, most of the fitting lines at the later stage deviated from the experimental data. Therefore, it was believed that the deviations were caused by the interference of chemical reactions with molecular diffusion in the near-equilibrium region.

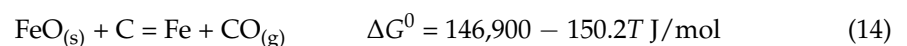
Using $(1 - 2\alpha/3 - (1 - \alpha)^{2/3}) = f(\alpha)_{\text{test point}}$ and $k't = f(\alpha)_{\text{fitting point}}$ in Equation (3) as the experiment value and the equation-fitting value, respectively, Equation (12) becomes Equation (13):

$$J_{\text{interference}} = \frac{\Delta f(\alpha)}{\Delta t} = \frac{f(\alpha)_{\text{test point}} - f(\alpha)_{\text{fitting point}}}{\Delta t} = l_1 \frac{A}{T} + l_2 \left(\frac{A}{T}\right)^2 + l_3 \left(\frac{A}{T}\right)^3 + \dots \quad (13)$$

where $J_{\text{interference}}$ is the mass-transfer flux when there is interference of a chemical reaction with molecular diffusion in the near-equilibrium region ($1/t$); $\Delta f(\alpha)$ is the difference between the later-stage molecular-diffusion experimental data and the fitting value in Figure 3b,d,f,h; Δt is the unit time in minutes, l_i is the diffusion coefficient of the chemical reaction (mutual phenomenological coefficient) in mole-Kelvin per Joule-minute; A is the affinity (the chemical potential difference between the products and the reactants in joules per mole); and T is the reaction temperature in Kelvin.

First, the $\Delta f(\alpha)$ values corresponding to different moments were determined, as shown in Figure 3b,d,f,h. Second, the change rate per unit time ($\Delta f(\alpha)/\Delta t$) was calculated, and then the calculated value of $\Delta f(\alpha)/\Delta t$ was plotted against A/T . Finally, the diffusion coefficient of chemical reaction l_i and the order of the higher-order polynomial could be obtained during diffusion at the later stage in the near-equilibrium region.

According to the principle of step-by-step reaction, iron oxides in the sinter were reduced by CO to form CO_2 , whereas CO_2 reacted with C to form CO in the presence of excess coke in the upper thermal reserve lump zone of the blast furnace. The coupling reaction is presented as follows:



$$\frac{A}{T} = \frac{\Delta G^0}{T} + R \ln \frac{a_{\text{Fe}} P_{\text{CO}}}{a_{\text{FeO}} a_{\text{C}}} = \frac{146,900}{T} - 150.2 + R \ln P_{\text{CO}} \quad (15)$$

At any moment at the later stage of FeO reduction, A/T could be determined by substituting the measured CO value and its corresponding temperature (1273 K) into Equation (15).

Figure 5 shows the fitting curves of different orders of high-order polynomials between $\Delta f(\alpha)/\Delta t$ and A/T in different experiments.

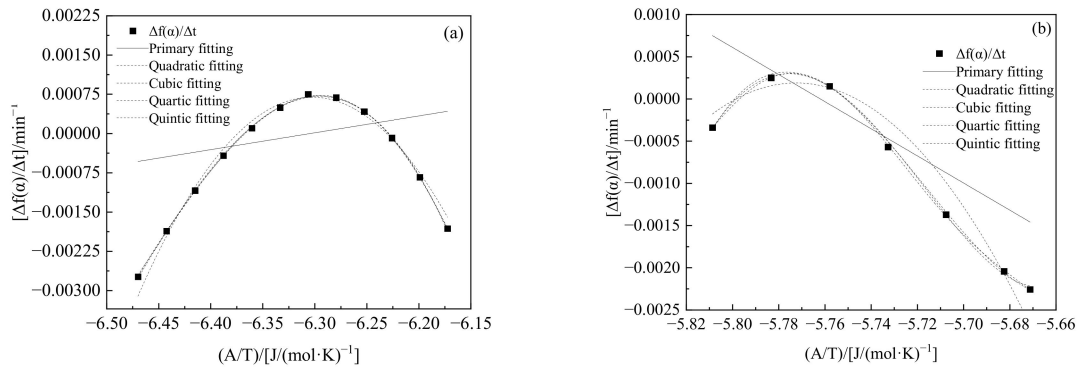


Figure 5. Fitting curves of different orders of high-order polynomials. (a) Fitting curve of different orders of high-order polynomials in experimental scheme 1-3; (b) fitting curve of different orders of high-order polynomials in experimental scheme 2-1.

As shown in Figure 5, the formulas of different orders of high-order polynomials, which were fitted by Equation (13), are as shown in Table 7 (where $x = (A/T)$).

Table 7. Fitted equations and the correlation coefficient of different orders of polynomials.

Fitted Equation	Sample 1-3	Correlation Coefficient r_3 of 1-3	Sample 2-1	Correlation Coefficient r_3 of 2-1
Second-order equation	$-5.3859 - 1.7093x - 0.1356x^2$	0.9872	$-9.3249 - 3.2309x - 0.2798x^2$	0.9556
Third-order equation	$-53.63 - 24.63x - 3.7652x^2 - 0.1915x^3$	0.9991	$588.92 + 309.10x + 54.07x^2 + 3.1527x^3$	0.9924
Fourth-order equation	$565.62 + 367.76x + 89.47x^2 + 9.6538x^3 + 0.3898x^4$	0.9995	$62032.58 + 42866.91x + 11107.63x^2 + 1279.09x^3 + 55.23x^4$	0.9969
Fifth-order equation	$39753.62 + 31379.97x + 9905.69x^2 + 1563.10x^3 + 123.305x^4 + 3.8897x^5$	0.9996	$-7.7017 - 6.7160x - 2.3424x^2 - 408497.84x^3 - 35616.78x^4 - 1242.11x^5$	0.9996

Figure 5 shows that the error of the first-order equation was large, indicating that the effect of chemical reactions on the mass transfer and diffusion was not linear, and a higher-order polynomial had to be considered. The fitting result of the second-order equation was greatly improved, but it was not as good as that of the third-order equation. With the increase of the order of the higher-order polynomial, the correlation coefficient increased and reached more than 0.990. Therefore, a third-order polynomial equation could be adopted. This was consistent with the findings of a previous study on the kinetics of reaction using a nonequilibrium thermodynamic method that adopted a third-order polynomial equation [30]. In this way, fitting results not only maintained a relatively high accuracy, but also ensured the equation was not significantly complicated.

4.3. Improvement of Mass-Transfer and Diffusion Equation during Sinter Reduction

As shown in Figure 5, the constant term existed in the formulas of different orders of high-order polynomials because the fitting curves were not through the origin (even if the high-order polynomials were through the origin). Considering the significance of the interference of chemical reactions on diffusion was the correction of the experimental point and fitting point, the constant term (also could be seen as the zero-order relationship of A/T) was introduced in Equation (16):

$$J_{\text{interference}} = \frac{\Delta f(\alpha)}{\Delta t} = \frac{f(\alpha)_{\text{test point}} - f(\alpha)_{\text{fitting point}}}{\Delta t} = l_0 + l_1 \frac{A}{T} + l_2 \left(\frac{A}{T}\right)^2 + l_3 \left(\frac{A}{T}\right)^3 + \dots \quad (16)$$

where l_0 is the constant term.

Table 8 shows the chemical-reaction and diffusion coefficients (third-order polynomial equation) considering the interference of chemical reactions on mass transfer and diffusion at the later stage of the reduction of FeO present in the sinter under different experimental conditions.

Table 8. Chemical-reaction and diffusion coefficients (third-order polynomial equation) at the later stage.

Sample No.	l_0	l_1	l_2	l_3	r_3	
1	1-1	−44.04	−20.04	−3.0325	−0.1525	0.9985
	1-2	232.04	117.22	19.73	1.1073	0.9972
	1-3	−53.63	−24.63	−3.7652	−0.1915	0.9991
2	2-1	588.92	309.10	54.07	3.1527	0.9924
	2-2	−85.85	−47.91	−8.9035	−0.5508	0.9998
	2-3	−21.43	−9.2661	−1.3346	−0.06406	0.9957
3	3-1	−23.01	−9.5325	−1.2983	−0.05793	0.9999
	3-2	10.11	5.2150	0.8910	0.0505	0.9957
	3-3	66.23	30.70	4.7428	0.2441	0.9980
4	−8.0952	−3.2416	−0.4224	−0.01777	0.9922	

According to the corresponding chemical-reaction and diffusion coefficients of different orders, as shown in Table 7, the improved mass-transfer and diffusion equation considering the coupling reaction at the later stage is as follows:

$$\left(1 - \frac{2}{3}\alpha - (1 - \alpha)^{\frac{2}{3}}\right) = \left\{k' + \left(l_0 + l_1 \frac{A}{T} + l_2 \left(\frac{A}{T}\right)^2 + l_3 \left(\frac{A}{T}\right)^3\right)\right\} t \quad (17)$$

The improved mass transfer and diffusion equation could be quantitatively obtained by substituting the corresponding data in Tables 6 and 7 into Equation (17). For example, Equation (18) is the improved mass-transfer and diffusion equation corresponding to experimental scheme 1-1 within the mass-transfer and diffusion control time.

$$\left(1 - \frac{2}{3}\alpha - (1 - \alpha)^{\frac{2}{3}}\right) = \left\{0.000778 + \left(-44.04 - 20.04 \frac{A}{T} - 3.0325 \left(\frac{A}{T}\right)^2 - 0.1525 \left(\frac{A}{T}\right)^3\right)\right\} t \quad (18)$$

3300 s ≤ t ≤ 7200 s

Similarly, the improved mass-transfer and diffusion equation of other experiments could be obtained. It is important to point out that the corresponding time frames of mass transfer and diffusion were different for different equations.

5. Conclusions

The kinetics of sinter reduction in the blast furnace block zone heat reserve was studied using a sectioning method suitable for the development of metallurgical reactions. According to the characteristics of sinter reduction in the presence of excess coke and different proportions of CO and CO₂ in the heat reserve area, the unreacted core model for controlling the speed of chemical reactions in the early stage and the internal-diffusion shrinkage core model for controlling the speed of the diffusion mass transfer in the later stage were established. The experimental data were fitted through the sectioning method, and the model was in good agreement with the experimental data. The kinetic parameters of the sinter reduction reaction in the heat reserve area were obtained.

The kinetic parameters obtained through the sectioning method allowed us to quantitatively discuss the effects of different conditions on sinter reduction. In addition, the kinetic models in the early and later stages of the reaction and the conversion time points of different control processes could be given quantitatively, and the necessary parameters in the definite solution conditions were provided for the simulation of a sinter-reduction reaction in the bulk zone heat reserve area of the blast furnace. When there were small changes in temperature, it could be considered that in the Arrhenius formula of the chemical-reaction-rate constant and molecular-diffusion coefficient in the heat reserve zone, the pre-exponential factor A , reaction-activation energy E_0 , standard-state diffusion coefficient D_0 , and diffusion-activation energy E were approximately constant. Other reaction-rate constants after temperature fluctuations in the heat reserve zone could be calculated from the reaction-rate constant and molecular-diffusion coefficient measured at 1000 °C.

The rate constant of the chemical reactions was three orders of magnitude higher than the molecular-diffusion coefficient, and the correlation coefficient in the early stage of reaction fitted by the model was higher than that in the late stage of reaction. It was necessary to consider the effect of the interference of chemical reactions on the mass transfer and diffusion in the late stage of sinter reduction (in the near-equilibrium region). Based on the basic principle of the thermodynamics of irreversible processes, a method to determine the interference of chemical reactions on mass transfer under the near-equilibrium condition was proposed, and the chemical-reaction and diffusion coefficients at the late stage of sinter reduction were determined (near equilibrium), which further improved the fitting degree of diffusion and mass-transfer model parameters, and improved the sectioning method suitable for the study of process dynamics in metallurgical reactions.

Author Contributions: Conceptualization, K.W. and W.Z.; methodology, L.Z.; software, Y.S.; validation, L.Z., W.Z. and K.W.; formal analysis, Y.L.; investigation, L.Z.; resources, L.Z.; data curation, L.Z.; writing—original draft preparation, K.W.; writing—review and editing, W.Z.; visualization, L.Z.; supervision, K.W.; project administration, W.Z.; funding acquisition, W.Z. All authors have read and agreed to the published version of the manuscript.

Funding: This research was funded by the National Natural Science Foundation of China (Nos. 51974154, 52074150 and 51604148).

Institutional Review Board Statement: Not applicable.

Informed Consent Statement: Not applicable.

Data Availability Statement: Not applicable.

Conflicts of Interest: The authors declare no conflict of interest.

References

1. Chen, Y.B.; Liu, W.G.; Chen, J.S.; Zuo, H.B. Gasification behavior of phosphorus during hydrogen-rich sintering of high-phosphorus iron ore. *ISIJ Int.* **2022**, *62*, 496–503. [[CrossRef](#)]
2. Zhang, X.; Wen, Z.; Lou, G.F.; Liu, X.L.; Zheng, K.C. Numerical simulation and parameters analysis on the gas-solid heat transfer process of high temperature sinter. *Chin. J. Eng.* **2011**, *33*, 339–345.
3. Wang, W.; Chen, X.H.; Xu, R.S.; Li, J.; Shen, W.J.; Wang, S.P. Research progress on multiscale structural characteristics and characterization methods of iron ore sinter. *J. Iron Steel Res. Int.* **2020**, *27*, 367–379. [[CrossRef](#)]
4. Takeuchi, N.; Iwami, Y.; Higuchi, T.; Nushiro, K.; Oyama, N.; Sato, M. Evaluation of sinter quality for improvement in gas permeability of blast furnace. *ISIJ Int.* **2014**, *54*, 791–800. [[CrossRef](#)]
5. El-Geassy, A.A. Gaseous reduction of MgO-doped Fe₂O₃ compacts with carbonmonoxide at 1173–1473 K. *ISIJ Int.* **1996**, *36*, 1328–1337. [[CrossRef](#)]
6. Murakami, T.; Kodaira, T.; Kasai, E. Reduction and disintegration behavior of sinter under N₂–CO–CO₂–H₂–H₂O gas at 773 K. *ISIJ Int.* **2015**, *55*, 1181–1187. [[CrossRef](#)]
7. Wu, K.; She, Y.; Zhu, L.; Zhan, W.L.; Liu, Q.H. Consideration on the subject system of metallurgical reaction engineering. *J. Iron Steel Res.* **2014**, *26*, 1–8.
8. Wu, K.; Zhang, J.Z.; Zhao, Y.; Zhu, L.; She, Y. Research methods on the reaction kinetics of metallurgical reaction engineering. *Nonferrous Met. Sci. Eng.* **2014**, *5*, 1–6.

9. Zhao, Y.; Wu, K.; Pan, W.; Liu, Q.H. Investigation of the reduction kinetics process of sinter ore by sectional stepwise method. *J. Nort. Univ. Nat. Sci.* **2013**, *34*, 1282–1287.
10. Huang, X.H. *Principles of Iron and Steel Metallurgy*; Metallurgical Industry Press: Beijing, China, 1990.
11. Angalakuditi, V.B.; Bhadravathi, P.; Gujare, R.; Ayyappan, G.; Singh, L.R.; Baral, S.S. Mineralogical Aspects of Reducing Lump Iron Ore, Pellets, and Sinter with Hydrogen. *Metall. Mater. Trans. B* **2022**, *53*, 1036–1065. [[CrossRef](#)]
12. She, Y.; Zhang, W.Z.; Zhan, W.L.; Zhu, L.; Wu, K. Kinetics mechanism of coke solution loss reaction in thermal reserve zone of blast furnace by modified sectioning method. *J. Cent. South Uni. Sci. Technol.* **2021**, *52*, 4227–4237.
13. Zhang, J.L.; Zhang, Y.P.; Li, K.J.; Wang, Y.Z.; Liu, Z.J.; Wang, G.W. Microstructure and phase transformation of a sinter bearing low Ti during reduction. *Metall. Mater. Trans. B* **2016**, *47*, 3046–3055. [[CrossRef](#)]
14. Hessling, O.; Fogelström, J.B.; Kojola, N.; Du, S.C. The effect of the endothermic reaction nature on the iron ore pellet reduction using hydrogen. *Mater. Trans. B* **2022**, *53*, 1258–1268. [[CrossRef](#)]
15. Dasgupta, S.; Saleem, S.; Srirangam, P.; Auinger, M.; Roy, G.G. A computational study on the reduction behavior of iron ore/carbon composite pellets in both single and multi-layer bed rotary hearth furnace. *Mater. Trans. B* **2020**, *51*, 818–826. [[CrossRef](#)]
16. Mousa, E.A.; Ghali, S. Factorial design analysis of reduction of simulated iron ore sinter reduced with CO gas at 1000–1100 °C. *Ironmak. Steelmak.* **2015**, *42*, 311–319. [[CrossRef](#)]
17. Wu, K.; She, Y.; Liu, Q.H.; Zhan, W.L. Consideration on properties of coke and coke deterioration after large-scale blast furnace. *Iron Steel* **2017**, *52*, 1–12.
18. Naito, M.; Takeda, K.; Matsui, Y. Ironmaking technology for the last 100 years: Deployment to advanced technologies from introduction of technological know-how, and evolution to next-generation process. *ISIJ Int.* **2015**, *55*, 7–35. [[CrossRef](#)]
19. Hessien, M.M.; Kashiwaya, Y.; Ishii, K.; Nasr, M.I.; El-Geassy, A.A. Characterisation of iron ore sinter and its behaviour during non-isothermal reduction conditions. *Ironmak. Steelmak.* **2008**, *35*, 183–190. [[CrossRef](#)]
20. Liu, Q.H.; Yang, S.P.; Wang, C.; Ji, Y.L. Effect of carbon solution-loss reaction on properties of coke in blast furnace. *J. Iron Steel Res. Int.* **2020**, *27*, 489–499. [[CrossRef](#)]
21. Ling, Q.; Zhao, H.J.; Chen, L.Y.; Xie, R.L.; Lei, Z.; Zhao, Z.G.; Cui, P. A comparison study of existence forms of Fe species in coke for solution loss reaction of carbon. *J. Iron Steel Res. Int.* **2018**, *25*, 692–699. [[CrossRef](#)]
22. Chang, Z.Y.; Jiao, K.X.; Zhang, J.L.; Ning, X.J. Insights into accumulation behavior of harmful elements in cohesive zone with reference to its influence on coke. *ISIJ Int.* **2019**, *59*, 1796–1800. [[CrossRef](#)]
23. Mizoguchi, H.; Suzuki, H.; Hayashi, S. Influence of Mixing Coal Composite Iron Ore Hot Briquettes on Blast Furnace Simulated Reaction Behavior in a Packed Mixed Bed. *ISIJ Int.* **2011**, *51*, 1247–1254. [[CrossRef](#)]
24. Degroot, S.R.; Mazur, P. *Non-Equilibrium Thermodynamics*; North-Holland Publishing Company: Amsterdam, The Netherlands, 1962.
25. Peng, S.; Zhang, Z. *The Progress and Application of Linear and Nonlinear Non-Equilibrium Thermodynamics*; Chemical Industry Press: Beijing, China, 2006.
26. Zhai, Y.C. *Non-Equilibrium Thermodynamics*; Science Press: Beijing, China, 2015.
27. Zhang, L.; Wu, K.; Du, R.L.; Chao, C.Y.; Xu, D.A. A sectioning method to study the gasification reaction kinetics of semicoke with CO₂. *Chin. J. Eng.* **2016**, *38*, 1539–1545.
28. Du, R.L.; Wu, K.; Xu, D.A.; Chao, C.Y.; Zhang, L.; Du, X.D. A modified Arrhenius equation to predict the reaction rate constant of Anyuan pulverized-coal pyrolysis at different heating rates. *Fuel Process. Technol.* **2016**, *148*, 295–301. [[CrossRef](#)]
29. Wang, W.Z.; Zhan, W.L.; Liu, X.; Liu, Q.H.; Yu, Y.C.; Wu, K. High temperature reaction characteristics of coke in blast furnace. *Nonferrous Met. Sci. Eng.* **2014**, *5*, 9–13.
30. Zhai, Y.C.; Wang, J.X. Study of manganese oxide reduction in slag-metal phase through thermodynamics of irreversible process. *Acta Metall. Sin.* **2004**, *40*, 305–308.